Nuclear Wave Packet Motion between P* and $P^+B_A^-$ Potential Surfaces with a Subsequent Electron Transfer to H_A in Bacterial Reaction Centers at 90 K. Electron Transfer Pathway†

Andrei G. Yakovlev,‡ Anatoli Ya. Shkuropatov,§ and Vladimir A. Shuvalov*,‡,§

Department of Photobiophysics, Belozersky Institute of Chemical and Physical Biology, Moscow State University, Moscow 119992, Russia, and Institute of Basic Biological Problems, Russian Academy of Sciences, Pushchino, Moscow Region 142290, Russia

Received March 29, 2002; Revised Manuscript Received July 15, 2002

ABSTRACT: In *Rhodobacter sphaeroides* R-26 reaction centers (RCs) the nuclear wave packet induced by 25 fs excitation at 90 K moves on the primary electron donor P* potential energy hypersurface with initial frequency at ∼130 cm^{-1} (monitored by stimulated emission measurement). At the long-wavelength side of P* stimulated emission at 935 nm the wave packet is transferred to the surface with $P^+B_A^-$ character at 120, 380, 1.2 fs, etc. delays (monitored by measurement of the primary electron acceptor B_A^- band at 1020 nm). However, only beginning from 380 fs delay and later the relative stabilization of the state $P^+B_A^-$ is observed. This is accompanied by the electron transfer to bacteriopheophytin H_A (monitored by H_A band measurement at 760 nm). The most active mode of 32 cm^{-1} in the electron transfer and its overtones up to the seventh were found in the Fourier transform spectrum of the oscillatory part of the kinetics of the P* stimulated emission and of the $P^+B_A^-$ and $P^+H_A^-$ formation. This mode and its overtones are apparently populated via the 130 cm^{-1} vibrational mode. The deuteration of the sample shifts the fundamental frequency (32 cm^{-1}) and all overtones by the same factor of ∼1.3. This mode and its overtones are suppressed by a factor of ∼4.7 in the dry film of RCs. The results obtained indicate that the 32 cm^{-1} mode might be related to a rotation of hydrogen-containing groups (possibly the water molecule) participating in the modulation of the primary electron transfer from P* to B_A^- in at least 35% of RCs. The Brookhaven Protein Data Bank (1PRC) displays the water molecule located at the position HOH302 between His M200 (axial ligand for P_B) and the oxygen of ring V of B_A which might be a part (∼35%) of the molecular pathway for electron transfer from P* to B_A.

The photosynthetic bacterial reaction center (RC)[1] is a hexachromophoric protein responsible for the conversion of light energy into the free energy of the charge-separated states. The X-ray analysis of bacterial RCs has shown (*1*) that a local 2-fold rotational axis runs through two bacteriochlorophylls constituting the special pair P near the periplasmic side of the membrane and separates symmetrically two bacteriochlorophyll monomers (B_A and B_B) and two bacteriopheophytins (H_A and H_B) located in the hydrophobic central part of the membrane. Two branches (A and B) of the pigments are terminated by two quinones (Q_A and Q_B) near the cytoplasmic side of the membrane. Light-induced charge separation results in the formation of positive (P^+) and negative (Q^-) charges on opposite sides of the membrane. The separated charges are used for further biochemical processes in the cell. The structure of bacterial RCs is consistent with the sequence of the electron transfer reactions taking place between cofactors located in the A branch (*2*).

The question raised in the first (*3*) and second (present) parts of the work is related to the mechanism of the primary step of the light energy conversion into the energy of separated charges between the excited state of the primary electron donor P and the primary electron acceptor. On the basis of experimental data (*4*−*13*) B_A has been suggested to play a role of the primary electron acceptor, in agreement with its position between P and H_A in the X-ray model (*1*). Then the state $P^+B_A^-$ can be a first charge-separated state in which radical cation (P^+) and anion (B_A^-) have spectral properties close to those observed individually.

Other workers (*14*−*20*) argue that the sum of the experimental data can be better interpreted as an indication of the parallel possibilities for two-step ET and for the superexchange mechanism involving the vacant orbital of B_A for the ET from P* to H_A. In that respect the interesting data were obtained for Pheo-modified RCs (*8*, *9*) in which the interaction between P and B_A was unchanged but further electron transfer to H_A was blocked in the picosecond time domain. For these RCs the formation of the long-lived (∼1 ns) state $P^+B_A^-$ was observed with spectral properties close to the sum of those for P^+ and B_A^-. The 1020 nm band observed for this state was found to be characteristic for the

† Support by the Russian Basic Research Foundation (Grant N 02-04-48650), INTAS, and NWO (The Netherlands) is gratefully acknowledged. A preliminary account of this work has been presented at the XIIth conference on Ultrafast Processes in Spectroscopy, Florence, Italy, Oct 2001.

* To whom correspondence should be addressed. Fax: (7)(096) 7790532. E-mail: shuvalov@issp.serpukhov.su. Phone: (7)(096) 7733601.

‡ Moscow State University.

§ Russian Academy of Sciences.

[1] Abbreviations: Δ*A*, light-minus-dark absorbance changes; B_A and H_A, the primary and secondary electron acceptors, respectively, located in active branch A; RC, reaction center; ET, electron transfer; FT, Fourier transform; IR, infrared; P, primary electron donor; Pheo, plant pheophytin.

10.1021/bi020250n CCC: $22.00
Published on Web 10/31/2002

radical anion of bacteriochlorophyll (*8*, *9*). As shown in ref *3* the appearance of the 1020 nm band at a very earlier time (at 120 fs) strongly suggests that the state $P^+B_A^-$ is a first product of the charge separation. It was also found (*9*) that the B_A band bleaching at 800 nm corresponds stoichiometrically to the P band bleaching at 890 nm. The latter is not changed when P^*B_A is converted to $P^+B_A^-$. This indicates that all electron density is shifted from P* to B_A at picosecond delay. Furthermore, it was found (see ref *9*) that $P^+B_A^-$ has lower energy than P* and that very little admixture of superexchange is present in bacterial RCs.

The position of P_A, P_B, and B_A was determined by X-ray analysis in great detail (see Brookhaven Protein Data Bank, 1PRC) and shows several possibilities for the electron transfer pathway from P* to B_A. To check these possibilities, the frequency analysis of vibration and rotation of the groups involved in the charge separation can be applied.

Recent developments in femtosecond spectroscopy have provided a new tool for the nuclear dynamics study which is based on the finding that excitation of P by ultrashort (<30 fs) pulses of a broad spectral width creates a superposition of many vibrational wave functions known as a wave packet (*21*). The wave packet has a time-dependent position on the potential energy surface of P* and moves with the frequency corresponding to the energy difference between the vibrational levels involved. Such nuclear wave packet motions were visualized by the femtosecond oscillations in the kinetics of stimulated emission from P* (*22*−*25*). A displacement of the potential energy surface of P* with respect to that of P results in the time-dependent spectral position of the stimulated emission from P*. The long- and short-wavelength emission components are out of phase to each other but have similar oscillation frequencies. Fourier transform (FT) spectra of the oscillations show the oscillation modes at 15, 30, 69, 92, 122, 153, 191, and 329 cm^{-1} at 10 K (*24*), similar to those found in hole-burning experiments (*26*) and by Raman spectroscopy (*27*−*29*).

The primary step of the light energy conversion with involvement of coherent nuclear motions in the state P* was theoretically described in ref *30* by a harmonic bath model with the electronically diabatic (phonon) Hamiltonians for the ground (PB_A), locally excited (P^*B_A), and charge-separated ($P^+B_A^-$) states. The reaction coordinates Q_1 and Q_2 (*30*) were defined for the photoexcitation and the electron transfer processes, respectively. The angle (θ) between Q_1 and Q_2 determines the amplitude of femtosecond oscillations of the electron transfer rate treated by the Landau−Zener semiclassical approach: when $\cos\theta = -1$ (linear arrangement), the oscillations are maximal in the product; when $\cos\theta = 0$ (orthogonal arrangement), the oscillations are absent.

The results of the study of the coupling between primary charge separation and nuclear wave packet motions in bacterial RCs have shown that femtosecond oscillations are observed at 293 K in the dynamics of the population of the product state $P^+B_A^-$. This was monitored by measurements of absorption in the B_A band at 800 nm and the B_A^- absorption band at 1020 nm (*3*, *31*−*34*). These results are consistent with the angle θ close to 180° (linear arrangement of Q_1 and Q_2 coordinates). It was found that in RCs the wave packet is initially formed by femtosecond light pulses on the 130−140 cm^{-1} potential energy hypersurface of P*. The subsequent motion on this surface leads the wave packet to the intersection region between P* and $P^+B_A^-$ located close to the long-wavelength side (935 nm) of the stimulated emission band of P* (*3*, *31*−*34*). At 120 fs and mostly at 380 fs delays the wave packet reflects from the P* surface wall and is not stabilized onto the $P^+B_A^-$ surface at room temperature. The transmission coefficient is remarkably increased when the wave packet is transferred to the 32 cm^{-1} mode on the same P* hypersurface or on the mixed diabatic surface, part of which has $P^+B_A^-$ charge transfer character. The 32 cm^{-1} mode is enhanced with respect to others in the FT spectrum of the oscillatory part of the kinetics of the absorption development at 1020 nm, reflecting the $P^+B_A^-$ formation. The same is observed for the kinetics of the bleaching at 760 nm associated with the formation of $P^+H_A^-$.

Here we show that in bacterial RCs at 90 K the 32 cm^{-1} mode is probably related to the rotation of the water molecule which has higher harmonics up to seventh one in the stimulated emission from P*. This rotation modulates the electron transfer from P* to B_A as well. Therefore, it is suggested that one of the pathways for the electron transfer from P* to B_A might be along the bridge formed by polar groups according to the Brookhaven Protein Data Bank (1PRC): $Mg(P_B)$—N—C—N(His M200)—HOH—O═(B_A). Other possibilities for electron transfer are also discussed.

MATERIALS AND METHODS

RCs of *Rhodobacter sphaeroides* R-26 were isolated as described in ref *35*, and both native bacteriopheophytins (H_A and H_B) were exchanged with plant pheophytin *a* (Pheo) according to ref *5*. For studies at room temperature RCs were suspended in 10 mM Tris-HCl, pH 8.0/0.1% LDAO buffer. Low-temperature (90 K) measurements were performed on the samples containing 65% glycerol (v/v). To replace H_2O by D_2O, RCs suspended in H_2O buffer were concentrated on a membrane and then diluted by D_2O buffer. The dilution−concentration procedure was repeated twice. Such a treatment did not alter the absorption spectrum of RCs. The optical density of the samples was 0.5 at 860 nm at room temperature. Sodium dithionite (5 mM) was added to keep RCs in the state $PB_AH_AQ_A^-$.

A dry film of RCs was obtained by drying of the RCs solution at room temperature and relative humidity (∼40%) and then under vacuum conditions for 2 days. Before measurements the film was illuminated 300 times by 1064 nm laser microsecond pulses to evaporate residual water molecules. The absorption spectrum of RCs in the dry film was different from that in liquid by an ∼7 nm blue shift of the Q_Y band of P with a preservation of the Q_Y band of B_A.

Femtosecond transient absorption measurements were carried out with a home-built amplified Ti:sapphire laser system with continuum generation and optical multichannel analyzer detection, described in detail in ref *32*. The operating frequency was 15 Hz. The duration of pump and probe pulses was about 25 fs. Pump pulses were centered at 870 nm. The pump and probe pulses had a weak (∼20%) mutual perpendicular polarization while the remaining part (∼80%) was depolarized. The delay between pump and probe pulses was changed with an accuracy of ∼10 fs. The compression of temporal dispersion in the range from 600 to 900 nm was monitored by kinetics measurements at 600 nm (Q_x transition of P) and at 900 nm (Q_y transition of P and the short-

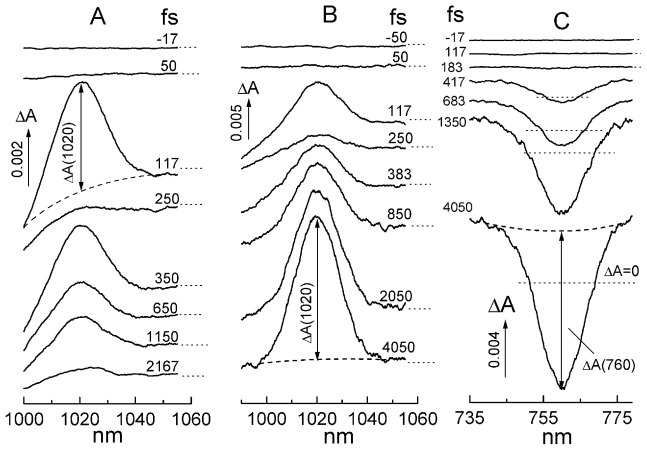

FIGURE 1: Difference (light-minus-dark) absorbance spectra acquired at various femtosecond delays at 90 K in native (A, C) and pheophytin-modified (B) *Rb. sphaeroides* R-26 RCs in glycerol−H_2O buffer excited by 25 fs pulses at 870 nm: (A, B) 990−1060 nm range (spectra of the $P^+B_A^-$ state); (C) 735−776 nm range (spectra of the $P^+H_A^-$ state). The double-headed arrows show amplitudes of the absorbance changes (ΔA) for spectral bands at 1020 and 760 nm superimposed on the broad spectral background. These amplitudes were used for kinetics plots (see Figures 2−6). The same was done for the stimulated emission band at 935 nm (not shown). The spectra of the 760 nm band bleaching are very similar to those presented for *Rb. spaeroides* R-26 RCs at 10 K by Vos et al. (*41*).

wavelength side of stimulated emission from P*). It was determined to be less than 50 fs. Out of phase oscillation at 900 and 935 nm observed earlier in refs *22*−*25* and in this work indicated that in this region the temporal dispersion was compressed to less than 10 fs. In-phase oscillation in the kinetics of absorbance changes at 935 and 1020 nm shown earlier (*32*−*34*) is consistent with the compression to less than 30 fs in the 930−1040 nm region. In agreement with these estimates the spectral band of the green glass filter (ZC-10; LOMO, St. Petersburg) in the range of 935−1060 nm was found to bleach within 30 fs without any changes of the shape of the band.

Transient absorption difference spectra were obtained by averaging of 3000−7000 measurements at each time delay. The accuracy of absorbance measurements was $(1-2) \times 10^{-4}$ units of optical density. The amplitude of the spectral bands at 1020, 760, and 935 nm (not shown) at different delays superimposed on the broad background was measured at their maxima as shown by double-headed arrows in Figure 1. The kinetics of absorbance changes (ΔA) at 1020, 935, and 760 nm were plotted using the measured amplitudes. The nonoscillating fits were subtracted from the kinetics, and the residual oscillatory parts of the kinetics were Fourier transformed (FT) to obtain the frequency spectra of oscillations. The fits correspond to a minimal amplitude of the oscillations. Uncertainty of the FT peaks is caused by an ordinate noise, the level of which is indicated for each FT spectrum in the text. The abscissa uncertainty of ± 4 cm^{-1} is related to the width of the measurement window (4.3 ps). Since the oscillations disappear within this time the artificial increase of the window (additional zero points after 4.3 ps) would not change experimental data but decrease the abscissa uncertainty. This approach has shown that the position of the major peaks is preserved in FT spectra and depends mostly on the average numbers of the measurements.

RESULTS

Femtosecond oscillations in stimulated emission from the primary electron donor excited state P* has been shown to be a result of the coherent nuclear motion within the single electronic state of P*****, which includes a possible contribution of various configurations (*3*, *22*−*25*, *31*−*34*). This is different from femtosecond oscillations observed in the charge-separated states $P^+B_A^-$ and $P^+H_A^-$. Panels A and B of Figure 1 show the absorption difference spectra of the 1020 nm band formation [B_A^- band (*3*, *7*−*13*, *32*−*34*)] at different delays at 90 K in native and Pheo-modified *Rb. sphaeroides* R-26 RCs, respectively. One can see the absence of any changes in the band shape and maximum position for a whole period of the measurements (0−4 ps). This observation suggests that the optical transition from B_A^- to $(B_A^-)^*$ is not altered at all delays used. Therefore, the femtosecond oscillations observed in the kinetics of the 1020 nm band development (see Figure 3) seem to be caused by coherent motions between different electronic states (most probably P* and $P^+B_A^-$) rather than by oscillations generated within only the product state.

Invariability of the band shape and maximum position of the bleaching of the bacteriopheophytin H_A absorption band at 760 nm at different delays in native RCs at 90 K shows (Figure 1C) that an electron is accepted by the same bacteriopheophytin molecule (H_A) in the same surroundings at all delays. On this basis femtosecond oscillations in the kinetics of the bleaching at 760 nm can be explained in terms of a coherent component in the dynamics of the population of the $P^+H_A^-$ state from a precursor state (most probably $P^+B_A^-$). No oscillations generated within the single $P^+H_A^-$ state appear to be present.

The double-headed arrows in Figure 1 demonstrate the approach we used to measure the amplitudes of the 1020 nm band development (B_A^- formation) and the 760 nm band bleaching (H_A^- formation) superimposed on the broad background. This background results from P*-stimulated emission near 1020 nm and from P* and $P^+B_A^-$ absorption increases near 760 nm, respectively. The amplitudes obtained in this way at different time delays were employed to obtain the kinetics of the different processes studied. The same was done for the 935 nm band, reflecting the P*-stimulated emission (see refs *3* and *32*−*34*).

Femtosecond Oscillations in Pheo-Modified RCs at 90 K. Figures 2A and 3A, dashed curves, show that in Pheo-modified RCs the decay of the P*-stimulated emission at 935 nm and the development of the B_A^- at 1020 nm occur at 90 K within ~1.5 ps, in agreement with ref *9*. Since the measurements in ref *9* have been done in the presence of oxidized Q_A, the reduction of Q_A performed in the present work does not change significantly the rate of the charge separation between P* and B_A. Superimposed on the nonoscillating exponential part of the kinetics, the femtosecond oscillations are observed both in the P*-stimulated emission decay and in the B_A^- development. After subtraction of nonoscillating components the oscillatory parts are presented in Figures 2B and 3B (dashed curves). The maximal amplitude of the oscillatory part is about 35% of the total absorbance changes. Fourier transform (FT) spectra of the oscillating components of the kinetics for Pheo-modified RCs are presented in Figures 2C and 3C (dashed

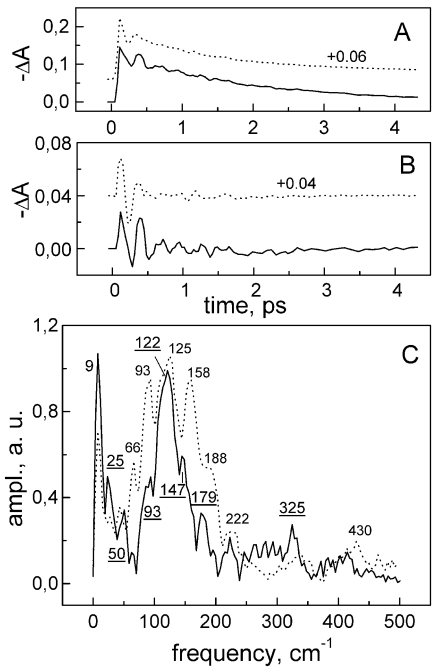

FIGURE 2: Femtosecond kinetics of ΔA (A), its oscillatory part (B), and the spectrum of Fourier transform of the oscillatory part (C) for the 935 nm band of pheophytin-modified R-26 RCs in glycerol−H_2O buffer (dashed curves) and in dry film (solid curves) at 90 K. RCs were excited by 25 fs pulses at 870 nm. Nonunderscored numbers in (C) show the characteristic frequencies of FT spectra of RCs in glycerol−H_2O buffer while underscored numbers show the analogous frequencies of RCs in dry film.

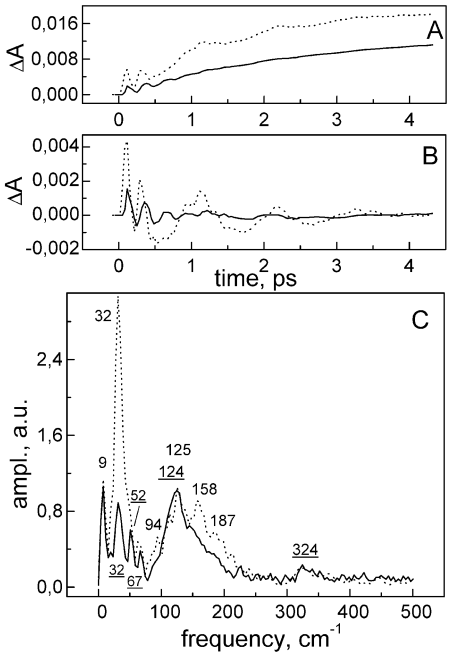

FIGURE 3: Femtosecond kinetics of ΔA (A), its oscillatory part (B), and the spectrum of Fourier transform of the oscillatory part (C) for the 1020 nm band in pheophytin-modified R-26 RCs in glycerol−H_2O buffer (dashed curves) and in dry film (solid curves) at 90 K. RCs were excited by 25 fs pulses at 870 nm. Nonunderscored numbers in (C) show the characteristic frequencies of FT spectra of RCs in glycerol−H_2O buffer while underscored numbers show the analogous frequencies of RCs in dry film.

curves). The level of noise for these spectra was estimated to be less than 0.02−0.04 of units used in the figures. The 32 cm^{-1} oscillations dominate in the 1020 nm kinetics, in agreement with measurements performed on Pheo-modified and native RCs at room temperature (*3*, *31*−*34*). In accordance with room temperature measurements (*3*) the overtones of the 32 cm^{-1} mode, found at 65−66, 93−94, 125−126, 158, 187−188, and 222−224 cm^{-1} (calculated as 64, 96, 128, 160, 192, and 224 cm^{-1}), are seen in both kinetics at 90 K as well. These observations agree well with the results of earlier measurements of oscillations in the kinetics of P*-stimulated emission at 10 K (*23*). Note that overtones are more intense in the P*-stimulated emission kinetics, whereas the fundamental 32 cm^{-1} frequency dominates in the kinetics of the B_A^- band development at 1020 nm (Figures 2C and 3C, dashed curves).

The appearance of the higher harmonics (up to the seventh one) in the P*-stimulated emission oscillation (Figures 2 and 3) is not characteristic of vibrational modes. Most probably, these oscillations are related to a rotation of small molecules such as OH^- or H_2O connected by a weak hydrogen bond to the photochemically active chromophores. To check this possibility, the kinetics at 935 and 1020 nm were measured in dry film of Pheo-modified RCs at 90 K (Figures 2 and 3, solid curves). Despite small changes in the dimer P absorption band after drying (see Materials and Methods and Discussion), the amplitude of the absorbance changes at 935 nm and their initial oscillations in dry film at 90 K are similar or even larger than in liquid (Figure 2A,B). In panel C the level of noise in these measurements was higher and was estimated to be less than 0.06−0.07 of units used. The overtone frequencies at 66, 93, 158, and 188 cm^{-1} seen in liquid are strongly suppressed in dry film (Figure 2C). Only a mode at 125 cm^{-1}, which has probably vibrational nature, is not changed in amplitude. The FT peak with the fundamental frequency at 32 cm^{-1} is well discernible in the 1020 nm kinetics in dry film, but its amplitude is decreased by a factor of ∼4.7 relative to that in liquid (Figure 3C). This occurs together with a decrease of amplitudes of the overtones with frequencies at 94, 158, and 187 cm^{-1}. Again, only the amplitude of the 125 cm^{-1} mode is preserved. Thus, femtosecond oscillations in the dimer (at 935 nm) and in $P^+B_A^-$ (at 1020 nm) become more simple upon drying and reflect mostly the (vibrational) mode at 125 cm^{-1} in both kinetics. These results are consistent with a possible assignment of the 32 cm^{-1} mode and its overtones to rotation of a water molecule, assuming that this molecule leaves the RCs during the drying procedure (see Materials and Methods). The level of final formation of the state $P^+B_A^-$ is decreased in dry film by a factor of 1.6 with respect to that in liquid (Figure 3A) that corresponds to the stop of ET in about 35% of RCs in the dry preparation. The lifetime of P* and the rise time of $P^+B_A^-$ in photochemically active RCs (∼65%) are increased in dry film up to 2.1−2.3 ps.

Femtosecond Oscillations in Native RCs at 90 K. The femtosecond kinetics similar to those described for Pheo-modified RCs are observed for the P*-stimulated emission at 935 nm in native RCs at 90 K (Figure 4). Despite the presence of efficient electron transfer to H_A the oscillations are present (Figure 4B) and superimposed on the exponential decay (∼1.5 ps lifetime), similar to that found for Pheo-modified RCs (Figure 2A). This finding suggests that the mechanism of the electron transfer process between P* and B_A is the same in native and Pheo-modified RCs. In Figures 4C and 5C the level of noise was estimated to be less than

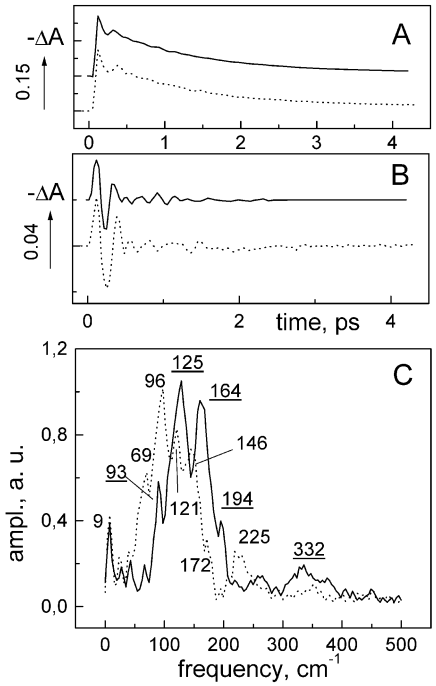

FIGURE 4: Femtosecond kinetics of Δ*A* (A), its oscillatory part (B), and the spectrum of Fourier transform of the oscillatory part (C) for the 935 nm band in native R-26 RCs at 90 K. Glycerol−H_2O buffer (solid curves) and glycerol−D_2O buffer (dashed curves) were used. RCs were excited by 25 fs pulses at 870 nm. Underscored numbers in (C) show the characteristic frequencies of FT spectra of RCs in glycerol−H_2O buffer while nonunderscored numbers show the analogous frequencies of RCs in glycerol−D_2O buffer.

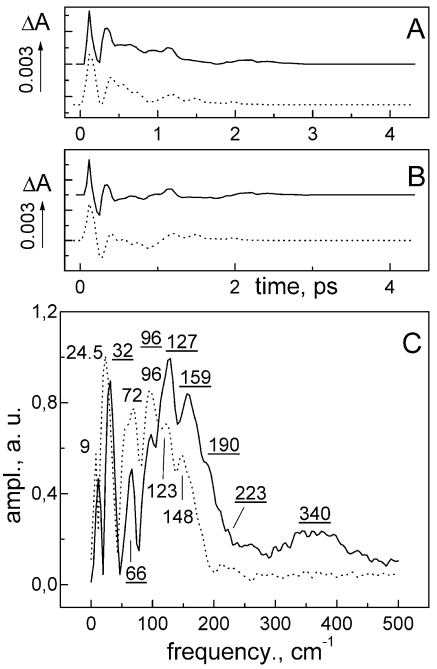

FIGURE 5: Femtosecond kinetics of Δ*A* (A), its oscillatory part (B), and the spectrum of Fourier transform of the oscillatory part (C) for the 1020 nm band in native R-26 RCs at 90 K. Glycerol−H_2O buffer (solid curves) and glycerol−D_2O buffer (dashed curves) were used. RCs were excited by 25 fs pulses at 870 nm. Underscored numbers in (C) show the characteristic frequencies of FT spectra of RCs in glycerol−H_2O buffer while nonunderscored numbers show the analogous frequencies of RCs in glycerol−D_2O buffer.

0.033 of units used in the figures. The frequencies of oscillations at 67, 93, 125, 164, and 194 cm^{-1} in the 935 nm kinetics in native RCs (Figure 4C) are very similar to those in Pheo-modified RCs (Figure 2C) and can also be assigned to the wave packet overtones of the 32 cm^{-1} mode.

The femtosecond oscillations, superimposed on the nonoscillating part of the kinetics at 1020 nm, are also observed for native RCs at 90 K (Figure 5A). This kinetics is, however, significantly different from that observed for Pheo-modified RCs. Indeed, in Pheo-modified RCs at 90 K the accumulation of the state $P^+B_A^-$ is observed within 1.5 ps. In native RCs such an accumulation is absent due to fast electron transfer from B^- to H_A (*36*). The development and decay of the population of $P^+B_A^-$ within first 2 ps are observed in native RCs. Interestingly, the 1020 nm peaks found at 120 and 380 fs delays are similarly observed in Pheo-modified and native RCs (Figures 3A and 5A). The oscillation peak at 1 ps is decreased, and peaks at 2 and 3 ps are very weak in native RCs. This is consistent with the efficient electron transfer from B_A^- to H_A during these time delays at 90 K (see Figure 6). The Fourier transform spectrum for native RCs (Figure 5C) includes the 32 cm^{-1} mode as a main component with its overtones.

To clarify the nature of the 32 cm^{-1} mode and its overtones in oscillations of the 935 and 1020 nm kinetics, the H_2O buffer was replaced by washing RCs in D_2O buffer (see Materials and Methods). Figures 4 (dashed curves) and 5 (dashed curves) show the effect of such a replacement on the oscillatory parts of the kinetics and their FT spectra. The central part of the FT spectrum for the 935 nm kinetics observed in H_2O buffer is shifted to lower frequencies in D_2O buffer by a factor of ∼1.3 (Figure 4C). Taking this factor into account, one can calculate the expected shift of the frequencies of the 32 cm^{-1} mode and its overtones: 24.5 cm^{-1} (instead of 32 cm^{-1}), 49.2 cm^{-1} (instead of 64 cm^{-1}), 73.8 cm^{-1} (96 cm^{-1}), 98.4 cm^{-1} (128 cm^{-1}),123 cm^{-1} (160 cm^{-1}), 147.7 cm^{-1} (192 cm^{-1}), and 172.3 cm^{-1} (224 cm^{-1}). The frequencies at 24.5, 69, 96, 121, 146, and 172 cm^{-1} are observed in FT spectra of RCs in D_2O buffer (Figure 4C). These frequencies are very close to calculated ones, which suggests their connection to the fundamental frequency of 32 cm^{-1} that is shifted by the same factor of ∼1.3 (Figures 4C and 5C). In fact, the main component at 32 cm^{-1} observed in the FT spectrum of femtosecond oscillations at 1020 nm and 90 K in native RCs is shifted to 24.5 cm^{-1} when H_2O is replaced by D_2O (Figure 5C). Other frequencies observed in the 1020 nm kinetics at 72, 96, 123, and 148 cm^{-1} in D_2O buffer are also consistent with the isotopic shift of overtones by a factor of ∼1.3.

The femtosecond oscillations superimposed on the nonoscillating part are also observed in the kinetics of H_A^- formation at 760 nm in native RCs at 90 K (Figure 6). The bleaching at 760 nm is almost absent during the development of the 1020 nm peak at 120 fs. Simulation shows that near 380 fs and 1.2 ps the 760 nm kinetics represents the integration of the B_A^- (1020 nm) peaks at 380 fs and 1.2 ps over time. These features are expectable if the appearance of the wave packet on the $P^+B_A^-$ surface leads to effective electron transfer to H_A proportionally to the time of the wave packet being on the $P^+B_A^-$ surface. In contrast to low-temperature measurements the electron transfer from B_A^- to H_A at room temperature has a lag phase (Figure 6A). The appearance of the B_A^- (1020 nm) peak at 380 fs is not accompanied by electron transfer from B_A^- to H_A in this case. Only the

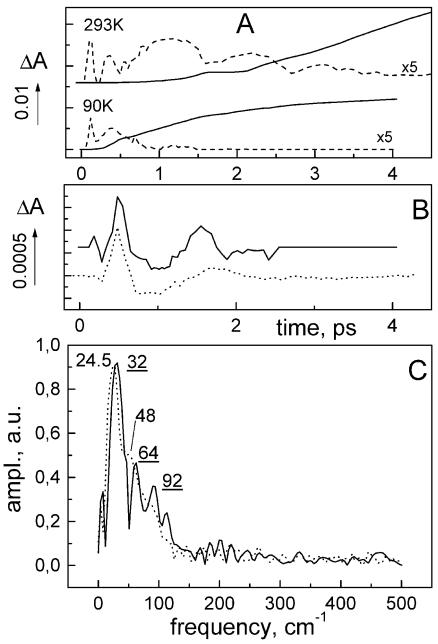

FIGURE 6: (A) Kinetics of Δ*A* in native R-26 RCs at 760 nm (solid curves) and 1020 nm (dashed curves) at 293 K (top curves) and 90 K (bottom curves). (B) Oscillatory parts of the kinetics at 760 nm in native RCs in glycerol−H_2O buffer (solid curve) and glycerol−D_2O buffer (dotted curve) at 90 K. (C) Fourier transform of the oscillatory parts of the 760 nm kinetics in native RCs in glycerol−H_2O buffer (solid curve) and glycerol−D_2O buffer (dotted curve). Underscored numbers in (C) show the characteristic frequencies of FT spectra of RCs in glycerol−H_2O buffer while nonunderscored numbers show the analogous frequencies of RCs in glycerol−D_2O buffer.

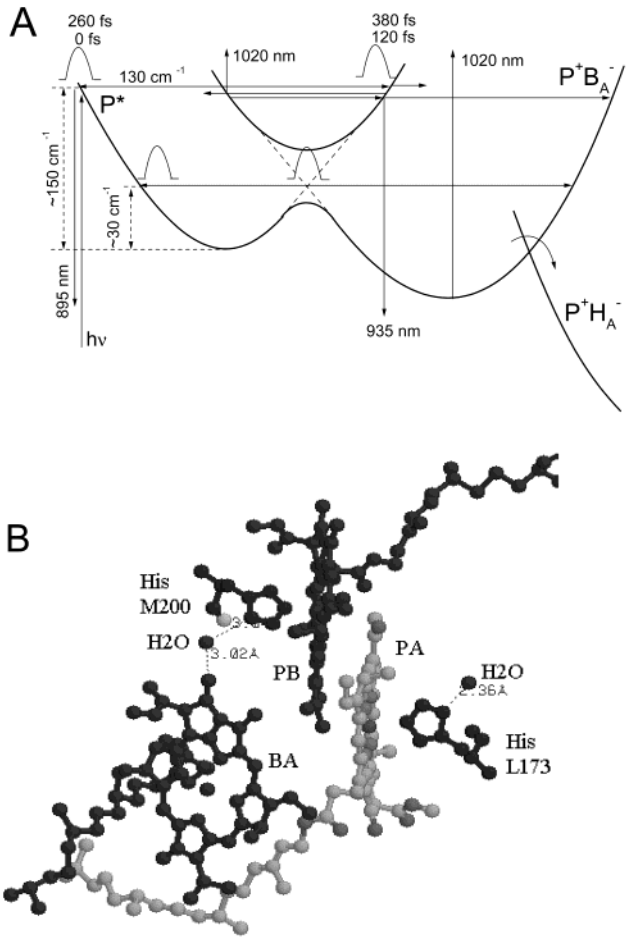

FIGURE 7: (A) Schematic representation (see refs *3* and *30*) of the diabatic (phonon) potential energy surfaces of the ground locally excited ($P^*B_AH_A$) and charge-separated ($P^+B_A^-H_A$ and $P^+B_AH_A^-$) states. An electronic coupling between P* and B_A splits two original surfaces (P* and $P^+B_A^-H_A$) into two upper and lower surfaces. The 130 cm^{-1} wave packet combined with the 32 cm^{-1} mode overtones can approach the upper part of the $P^*B_AH_A/P^+B_A^-H_A$ surface and produce emission at 935 nm (P*) and absorption at 1020 nm (B_A^-), indicated by arrows. The 32 cm^{-1} vibrational mode represents the wave packet motion on the lower part of the P*/$P^+B_A^-H_A$ surface. The $P^+B_AH_A^-$ surface is suggested to cross the lower part of the mixing surface having charge-separated character ($P^+B_A^-H_A$). (B) View (Brookhaven Protein Data Bank, 1PRC) of a special pair of bacteriochlorophylls P_A and P_B and monomeric bacteriochlorophyll B_A. His M200 liganding Mg of P_B is connected by a hydrogen bond via H_2O to the oxygen of the keto carbonyl group of ring V of B_A. Thus P_B is connected to B_A via a sequence of the following polar groups, Mg(P_B)—N—C—N(His M200)—H—O—H(water)—O═B_A, which can represent a pathway for the electron transfer from P* to B_A. The rotation of the water molecule in such a system with 32 cm^{-1} frequency is induced by the electron flow from P* to B_A (see text for details).

appearance of the B_A^- peaks at ∼1, ∼2, and ∼3 ps is accompanied by the electron transfer to H_A, but its efficiency is not as high as it is at low temperature for the 380 fs and 1 ps peaks.

The FT spectrum of the 760 nm kinetics at 90 K (Figure 6C) has a noise level less than 0.06 of units used. This spectrum includes a dominant band at 32 cm^{-1} and small bands at 64 and 92 cm^{-1}. All three bands are shifted to lower frequencies by a factor of ∼1.3 when H_2O buffer is replaced by D_2O buffer (Figure 6C). It should be noted that the FT spectrum for the 760 nm kinetics does not include frequencies around 130 cm^{-1} (Figure 6C). This is different from the FT spectra of the 935 and 1020 nm kinetics (Figures 4 and 5) and suggests that the 130 cm^{-1} mode and the 32 cm^{-1} mode overtones are not active in the wave packet transfer to the $P^+H_A^-$ potential energy surface.

DISCUSSION

A new tool for the study of electron−nuclear coupling during the femtosecond primary charge separation in bacterial RCs was developed recently by several groups (*3*, *11*, *22*−*25*, *31*−*34*). This approach is based on femtosecond spectroscopy, which allows to observe a quantum beat (coherence) related to the nuclear wave packet formation and the motion on the P* potential energy surface after femtosecond excitation of P with ultra-short (≤30 fs) light pulses.

The harmonic bath model for the electronically diabatic (phonon) Hamiltonians has been described in ref *30* for the ground (PB_A, H_1), locally excited (P^*B_A, H_2), and charge-separated ($P^+B_A^-$, H_3) states. The results of the application of such a model to femtosecond measurements were discussed in the first part of this work (*3*) in terms of the potential energy surfaces and their intercrossing (see Figure 7A). The nuclear wave packet motion on the 130 cm^{-1} potential surface of P* was found to be directly induced by light absorption (*26*) and to be along the reaction coordinate at room temperature (*3*, *32*−*34*). When the wave packet approaches the intercrossing area between P* and $P^+B_A^-$ potential energy surfaces at 120 and 380 fs delays, the intermediate mixed state emitting light at 935 nm (P*) and absorbing light at 1020 nm ($P^+B_A^-$) was observed. A slower motion of the wave packet on the 32 cm^{-1} surface was found

to be more effective for stabilization of $P^+B_A^-$ and for further electron transfer to H_A (Figure 7A).

The same results were obtained at low temperature in the present work. The similarities and differences of the 935 and 1020 nm kinetics at 90 K (Figures 2−5) can be interpreted in terms of two possibilities for electron transfer between P* and B_A (Figure 7A). According to Figure 7A an electronic coupling between P* and B_A splits two original surfaces (P* and $P^+B_A^-H_A$) into two upper and lower surfaces. The first possible ET occurs when the wave packet is located in the upper part of the intercrossing area between P* and $P^+B_A^-$ potential energy surfaces with simultaneous appearance of the P*-stimulated emission at 935 nm and B_A^- absorption band at 1020 nm at 120 fs and partially at 380 fs delays. The second possible ET occurs when the wave packet is transferred to the lower part of the intercrossing area at 380 fs and latter delays. The first case is realized at higher energy when the 125 cm^{-1} vibrational wave packet is combined with higher overtones of the 32 cm^{-1} mode. The second case is observed at lower energy of the 32 cm^{-1} mode and its lower overtones. The electron transfer from B_A^- to H_A seems to be only possible when the state $P^+B_A^-$ is formed according to the second case (Figure 6). It should be noted that the difference between the first and second cases is also related to a time period of the oscillations since the time is important for a reorganization of the surrounding molecular groups.

All kinetics and FT spectra presented in Figures 2−6 include oscillations with the fundamental frequency of 32 cm^{-1} and its overtones around 64 (second harmonics, 2), 96 (3), 128 (4), 160 (5), 192 (6), and 224 (7) cm^{-1}. The difference in the kinetics is mostly related to the different ratio between amplitudes of the fundamental oscillation and its overtones. For each electronic state this ratio can be explained in terms of efficiency and reversibility of further electron transfer: the more effective electron transfer and less reversibility, the smaller amplitude of the corresponding peak in the FT spectrum. An opposite situation takes place for the product: the more effective electron transfer and less reversibility, the larger amplitude of the peak in the FT spectrum of the product. From Figure 6C one can conclude that the most effective nuclear motion for total electron transfer from P* to H_A has a frequency at 32 cm^{-1}, in agreement with previous measurements (*3*, *25*, *32*−*34*). The same 32 cm^{-1} frequency is effective for stabilization of the first charge-separated state $P^+B_A^-$. Therefore, this mode is suppressed in the kinetics of the P* decay both in native and in Pheo-modified RCs. For the same reason the 32 cm^{-1} mode is enhanced in the $P^+B_A^-$ kinetics in Pheo-modified RCs but not so much in native RCs, in which further electron transfer to H_A takes place. Finally, this mode is a main one in the $P^+H_A^-$ kinetics in native RCs. In contrast, the higher overtones are not accompanied by effective stabilization of the $P^+B_A^-$ state. As a result, the enhanced overtones (3−6) are observed in the P* decay kinetics (Figures 2 and 4). Their amplitudes are smaller in the kinetics of the $P^+B_A^-$ formation (Figures 3 and 5), and almost no harmonics higher than 3 are present in the kinetics of the formation of $P^+H_A^-$ (Figure 6).

The appearances of the 1020 nm band seen in Pheo-modified RCs at 1.14, 2.17, and 3.2 ps are characterized by sine-like peaks (Figure 3B). These peaks are separated by an interval of ∼1.03 ps (32 cm^{-1}). Extrapolation of this series back to zero delay gives a value of ∼100 fs, which corresponds to the first oscillation peak in the P*-stimulated emission at 935 nm and in the B_A^- development at 1020 nm. However, at 120 fs delay there is a 1020 nm peak with much narrower width (∼100 fs) corresponding to that for the 935 nm emission from P* (125 cm^{-1} mode) (Figure 2C). This mode is clearly seen in dry film of RCs when the 32 cm^{-1} mode (Figure 3C) and its overtones (Figure 2C) are suppressed. We suggest therefore that the appearance of the wave packet in the intercrossing area between the P* and $P^+B_A^-$ potential energy surfaces at 120 fs (*34*) leads to the transformation of the 125 cm^{-1} mode (probably vibrational) into the 32 cm^{-1} mode and its overtones on the P* hypersurface. The higher overtones are populated in the 935 nm kinetics according to the energy difference between the 125 cm^{-1} vibrational mode and specific overtones of the 32 cm^{-1} mode (Figure 2C).

The nature of the 32 cm^{-1} mode and its overtones is of interest for further discussion. Usually, the presence of higher harmonics is not characteristic of vibrational modes. The appearance of several harmonics in P*- stimulated emission oscillations (Figure 2) might indicate that these oscillations are related to a rotation of small molecules such as OH^- or H_2O, located between the photochemically active RC chromophores. This assignment is tentative and does not exclude other possibilities. Another important point is related to the relative amplitude of oscillations (∼35%; see Figures 2 and 3). It means that all suggestions deal with this limited percentage of RCs.

In crystal structure of *Rhodopseudomonas viridis* RCs only two HOH molecules are known to be present between P and B_A and between P and B_B [see Brookhaven Protein Data Bank (1PRC) and ref *37*]. Based on the angle (∼104°) and distances between corresponding atoms (∼3 Å), it is reasonable to suggest that the water molecule, HOH302, can have a hydrogen bond to the N atom of His M200 (which serves as the axial ligand to magnesium of P_B) on the one side and to the keto carbonyl group of ring V of B_A on the other side (Figure 7B). Possible weakness or absence of the hydrogen bond between HOH and B_A observed by resonance Raman (see refs *27*−*29*) would be consistent with a rotation of HOH with parameters close to the gas phase. An alternative explanation might be that HOH rotation can occur after RC excitation when all hydrogen bonds of HOH (if they are existing) are broken.

It is known (*38*) that rotational spectra of small molecules in the gas phase include many lines reflecting the population of many harmonics. The rotational spectra of two-atom molecules are determined by the dipole electric moment. For $\Delta J = \pm 1$ and $\Delta K = 0$ (here J and K are quantum numbers) the infrared frequencies are determined as follows:

$$\nu = 2B(J+1) - 4D_j(J+1)^3 \qquad (1)$$

where B and D_j are rotational and centrifugal constants, respectively ($B \gg D_j$). The distance between infrared lines is equal to $2B$. The expression (eq 1) can be applied to an asymmetrical three-atom molecule like H_2O after some modification. For OH the B value is equal to 18.867 cm^{-1} and $\nu \sim 38$ cm^{-1} [in this case $4D_j(J+1)^3$ is suggested to be smaller than the first term in eq 1]. Three types of rotation of two protons around oxygen are possible for H_2O. To find

the ν values, one can use the B value for OH (18.867 cm^{-1}), equivalent mass (μ) for OH (0.941) and for H_2O (1.778) in which two protons are connected in one point, distances from O to H (0.9707 Å) and from H to the rotation axis (r), the angle between two bonds (104.5°), and the following expression for B:

$$B = h/(8\pi^2 c\mu r^2) \quad (2)$$

The calculated values of ν for H_2O are equal to ~32, ~52, and ~20 cm^{-1}. Notably, the 32 cm^{-1} mode and the frequency difference between two other modes (32 cm^{-1}) are equal to the 32 cm^{-1} mode observed in RCs. It is interesting that the 51−52 cm^{-1} mode was observed in RCs in which Q_A was doubly reduced (*31*) and in the dry film of RCs (Figure 3C).

On the basis of these estimates we suggest that peaks at 32, 66, 93, 125, 158, 188, and 222 cm^{-1} observed in the FT spectra of oscillations in the 935 nm and 1020 nm kinetics in Pheo-modified RCs (Figures 2C and 3C) are due to modulation of femtosecond kinetics by the rotation of the H_2O molecule. The same is probably true at room temperature (*34*). One can further suggest that the modulation is along the reaction coordinate of the primary charge separation reaction $P^* \rightarrow P^+B_A^-$ since all rotational frequencies are observed in oscillations of the kinetics of the B_A^- band development at 1020 nm.

The effect of isotopic exchange of HOH by DOD (or DOH) on the FT spectra (Figures 4−6) is consistent with these suggestions. The frequencies at 66, 93, 125, 164, and 194 cm^{-1} seem to belong to the higher harmonics of the 32 cm^{-1} mode, since all of these frequencies are shifted by the same factor of ~1.3 after H/D exchange. This finding indicates also that all these frequencies are related to the vibration or rotation of the H-containing groups. If the 125 cm^{-1} vibrational mode induces the 32 cm^{-1} mode overtones after light absorption, the question about isotopic shift of the 125 cm^{-1} mode arises. According to Figure 4C the frequency at 122 cm^{-1} seen in a dry film (Figure 2) is positioned just in the middle of the 32 cm^{-1} mode overtones after H/D exchange. Thus, the isotopic shift of the 125 cm^{-1} mode seems to be small. Probably, some anti-Stokes overtones seen in H_2O buffer are relatively enhanced due to a decrease of the first, second, and third harmonics induced by the electron transfer from P* to B_A. One can find from eq 2 that the magnitude of the isotopic shift for rotation induced by DOD/HOH exchange should be close to 1.9, which is larger than the factor of 1.3 found in our experiments. The simplest explanation of this discrepancy is a suggestion about an isotopic fractionation that does not allow complete replacement of both protons by deuterium in water molecules in the RC protein. In other words, the water molecule could be replaced by DOH instead of DOD. This effect is known for other isotopic exchange experiments (see ref *42*). Since measurements at 90 K were done in D_2O buffer with glycerol (65%) containing OH groups, the probability for HOH/DOH exchange may be higher than for HOH/DOD. In this case the factor of 1.4 can be found from calculations according to eq 2, which is close to the factor found experimentally. We do not exclude, however, that the discrepancy between the expected and observed effects points to a possibility of alternative interpretation of the results obtained. This work is in progress.

Figure 7B shows that in the RC of *R. viridis* (*1*, *37*) [the structure of which is very similar to that of *Rb. sphaeroides* RC (*39*)] "a bridge" is observed connecting P_B and B_A with the following elements (Brookhaven Protein Data Bank, 1PRC): (a) a coordination bond connecting Mg of P_B and N of His M200 (1.88 Å); (b) a hydrogen bond connecting another N of His M200 and an oxygen of HOH302; (c) a hydrogen bond connecting an oxygen of HOH302 and an oxygen of the keto carbonyl group of ring V of B_A. Distances are indicated by numbers. Using experimental data it is tempting to suggest that this bridge including the water molecule can be one of the possible pathways for ET from P* to B_A.

Using this assumption the sequence of the primary events can be tentatively described as follows. Before light absorption the bridge is in the dark state presented in Figure 7B and optimal for ET. Femtosecond excitation of P forms the nuclear vibration wave packet with the frequency of ~125 cm^{-1} (~270 fs) inside of P. The oscillating appearance of the stimulated emission from P* at 935 nm with a period of 270 fs can be explained as a consequence of an oscillating decrease of a distance between the porphyrin rings of P_A and P_B resulting in stronger exciton coupling between P_A and P_B with the admixing charge transfer state $P_B^{\delta-}P_A^{\delta+}$. This explanation is consistent with molecular orbital calculations which show that electron density is shifted from P_A to P_B (0.24/0.76) in the excited state P* (*40*). Furthermore, the electron density in P_B was found to be mostly located near the N atoms coordinating Mg in P_B (*40*). According to the X-ray model (*1*, *37*) these atoms are close to the nitrogen of His M200 liganding Mg in P_B. One can suppose that the electron density might be reversibly shifted from P* to B_A via the mentioned bridge when the wave packet appears [with the same initial time period (~270 fs)] in the intercrossing area between the P* and $P^+B_A^-$ surfaces, thus forming the state $P^+B_A^-$. This mechanism would be consistent with the reversible appearance of the B_A^- absorption band at 1020 nm at about 120, 390, 660, 930, 1200 fs, etc. (Figure 3). The rise times for the P*-stimulated emission at 935 nm and B_A^- band development at 1020 nm near 120 fs delay are different by 30 fs or less (Figures 2 and 3). This corresponds to an electron transfer velocity of $\geq 10^7$ cm/s. The electron transfer from P* to B_A is modulated by the 32 cm^{-1} mode (in liquid, but not in dry film) which has maxima for the 1020 nm band formation at 100, 1130, 2160, and 3190 fs and corresponding minima at 615, 1645, and 2675 fs (Figure 3). If the 32 cm^{-1} modulation is connected to the H_2O rotation, it means that the putative electron transfer bridge is destroyed and created again with a period of the H_2O rotation. The start of the H_2O rotation at ~100 fs correlates with the first shift of the electron density from P* to B_A. This shift seems to give an impulse for H_2O rotation. It is worth noting that the 270 fs oscillations seen in the P*-stimulated emission at 935 nm with peaks similar to the 1020 nm kinetic peaks at 120, 390, 660, 930, 1200 fs, etc. (Figure 2) are not modulated by the 32 cm^{-1} mode itself, being probably a result of combination of the 125 cm^{-1} mode with the 32 cm^{-1} mode overtones in liquid (Figure 2).

The results obtained here for the dry film of RCs can be compared with those described earlier (*43*−*45*). Despite some changes in the P spectral properties the primary photochemical reactions were observed. However, the electron transfer

rate was found to be decreased for different steps under dry conditions.

The primary step of charge separation is also suppressed in the dry film as one can see from Figures 2 and 3. We have already mentioned in the Results that the electron transfer from P* to B_A is blocked in about 35% of RCs in dry film. The amplitude of the 32 cm^{-1} peak in the FT spectrum of the same preparation is decreased by a factor of ~4.7 (Figure 3C). Taken together, these facts allow to suggest that (i) there are two populations of RCs and (ii) the modulation of the electron transfer from P* to B_A due to rotation of the HOH302 molecule takes place in a population of at least 35% of RCs from which this molecule is removable under drying conditions. Thus the capability of HOH for the rotation and evaporation seems to be correlated. It is important, however, that another (major) population of RCs appears to retain the ability to the charge separation in the dry film, only displaying some increase of the rise time of the $P^+B_A^-$ formation (from 1.5 ps in liquid to 2.1−2.3 ps in the dry film). One possible interpretation of these data is that there exist two entirely different, but equally effective, pathways for ET from P* to B_A but only one involves the water molecule. An alternative interpretation is that the water molecule is involved in ET in both populations of RCs but in major part HOH302 is stronger bounded. This does not allow the rotation and evaporation of HOH302. With this latter interpretation, modulation of ET from P* to B_A would not be functionally important although it provides an excellent opportunity to reveal a participation of the water molecule and clarify the possible pathway for ET in the primary photosynthetic electron transfer. Again, we should point out that suggested interpretation of the data obtained is one of possibilities and requires further investigation.

ACKNOWLEDGMENT

We thank Dr. A. V. Sharkov for help in maintenance of the femtosecond spectrometer and V. A. Shkuropatova for preparing the samples.

REFERENCES

1. Michel, H., Epp, O., and Deisenhofer, J. (1986) *EMBO J. 5*, 2445−2451.
2. Maroti, P., Kirmaier, C., Wraight, C., Holten, D., and Pearlstein, R. M. (1985) *Biochim. Biophys. Acta 810*, 132−141.
3. Yakovlev, A. G., Shkuropatov, A. Ya., and Shuvalov, V. A. (2002) *Biochemistry 41*, 2667−2674.
4. Shuvalov, V. A., Klevanik, A. V., Sharkov, A. V., Matveetz, Yu. A., and Krukov, P. G. (1978) *FEBS Lett. 91*, 135−139.
5. Arlt, T., Schmidt, S., Kaiser, W., Lauterwasser, C., Meyer, M., Scheer, H., and Zinth, W. (1993) *Proc. Natl. Acad. Sci. U.S.A. 90*, 11757−11761.
6. Shkuropatov, A. Ya., and Shuvalov, V. A. (1993) *FEBS Lett. 322*, 168−171.
7. Arlt, T., Schmidt, S., Kaiser, W., Lauterwasser, C., Meyer, M., Scheer, H., and Zinth, W. (1993) *Proc. Natl. Acad. Sci. U.S.A. 90*, 11757−11761.
8. Schmidt, S., Arlt, T., Hamm, P., Huber, H., Nagele, T., Wachtveitl, J., Meyer, M., and Scheer H. (1995) *Spectrochim. Acta, Part A 51*, 1565−1578.
9. Kennis, J. T. M., Shkuropatov, A. Ya., Van Stokkum, I. H. M., Gast, P., Hoff, A. J., Shuvalov, V. A., and Aartsma, T. J. (1997) *Biochemistry 36*, 16231−16238.
10. Arlt, T., Dohse, B., Schmidt, S., Wachtveitl, J., Laussermair, E., Zinth, W., and Oesterhelt, D. (1996) *Biochemistry 35*, 9235−9244.
11. Spörlein, S., Zinth, W., and Watchtveitl, J. (1998) *J. Phys. Chem. B 102*, 7492−7496.
12. Spörlein, S., Zinth, W., Meyer, M., Scheer, H., and Watchtveitl, J. (2000) *Chem. Phys. Lett. 322*, 454−464.
13. Beekman, L. M. P. (1997) Ph.D. Thesis (promoter, R. van Grondelle), VU, Amsterdam.
14. Marcus, R. A. (1989) in *The Photosynthetic Bacterial Reaction Center: Structure and Dynamics* (Breton, J., and Vermeglio, A., Eds.) pp 389−398, Plenum Press, New York and London.
15. Bixon, M., and Jortner, J. (1986) *J. Phys. Chem. 90*, *3795−3800*.
16. Kitzing, E., and Kuhn, H. (1990) *J. Phys. Chem., 94*, 1699−1715.
17. Parson, W. W., and Warshel, A. (1987) *J. Am. Chem. Soc. 109*, 6152−6163.
18. Breton, J., Martin, J.-L., Fleming, G. R., and Lambry J.-C. (1988) *Biochemistry 27*, 8276−8284.
19. Larsson, S., and Ivashin, N. V. (1999) *J. Appl. Spectrosc. 66*, 539−543.
20. Bixon, M., Jortner, J., Plato, M., and Michel-Beyerle, M. E. (1988) in *The Photosynthetic Bacterial Reaction Center: Structure and Dynamics* (J. Breton and A. Vermeglio, Eds.) pp 399−419, Plenum Press, New York and London.
21. Sokolov, A. A., Loskutov, Yu. M., and Ternov, I. M. (1962) *Quantum Mechanics*, Uchpedgiz, Moscow (in Russian).
22. Vos, M. H., Rappaport, F., Lambry, J.-C., Breton, J., and Martin, J.-L. (1993) *Nature 363*, 320−325.
23. Vos, M. H., Jones, M. R., McGlynn, P., Hunter, C. N., Breton, J., and Martin, J.-L. (1994*) Biochim. Biophys. Acta 1186*, 117−122.
24. Vos, M. H., Jones, M. R., Hunter, C. N., Breton, J., Lambry, J.-C., and Martin, J.-L. (1994) *Biochemistry 33*, 6750−6757.
25. Vos, M. H., Rischel, C., Jones, M. R., and Martin, J.-L. (2000) *Biochemistry 39*, 8353−8361.
26. Shuvalov, V. A., Klevanik, A. V., Ganago, A. O., Shkuropatov, A. Ya., and Gubanov, V. S. (1988) *FEBS Lett. 237*, 57−60.
27. Shreve, A. P., Cherepy, N. J., Franzen, S., Boxer, S. G., and Mathies, R. A. (1991) *Proc. Natl. Acad. Sci. U.S.A. 88*, 11207−11211.
28. Cherepy, N. J., Shreve, A. P., Moore, L. J., Franzen, S., Boxer, S. G., and Mathies, R. A. (1994) *J. Phys. Chem. 98*, 6023−6029.
29. Palaniappan, V., Aldema, M. A., Frank, H. A., and Bocian, D. F. (1992) *Biochemistry 31*, 11050−11058.
30. Ando, K., and Sumi, H. (1998) *J. Phys. Chem. B 102*, 10991−11000.
31. Streltsov, A. M., Vulto, S. I. E., Shkuropatov, A. Ya., Hoff, A. J., Aartsma, T. J., and Shuvalov, V. A. (1998) *J. Phys. Chem. B 102*, 7293−7298.
32. Yakovlev, A. G., Shkuropatov, A. Ya., and Shuvalov, V. A. (2000) *FEBS Lett. 466*, 209−212.
33. Yakovlev, A. G., and Shuvalov, V. A. (2000) *J. Chin. Chem. Soc. 47*, 709−714.
34. Yakovlev, A. G., Shkuropatov, A. Ya., and Shuvalov, V. A. (2001) in *Abstracts of the XIIth Conference on Ultrafast Processes in Spectroscopy*, p 13, UPS, Florence, Italy.
35. Shuvalov, V. A., Shkuropatov, A. Ya., Kulakova, S. M., Ismailov, M. A., and Shkuropatova, V. A. (1986) *Biochim. Biophys. Acta 849*, 337−348.
36. Lauterwasser, C., Finkele, U., Scheer, H., and Zinth, W. (1991) *Chem. Phys. Lett. 183*, 471−477.
37. Michel, H., and Deisenhofer, J. (1988) *Biochemistry 27*, 1−7.
38. Herzberg, H. (1949) *Vibrational and Rotational Spectra of Multiatoms Molecules*, Foreign Literature Publisher, Moscow.
39. Komiya, H., Yeates, T. O., Rees, D. C., Allen, J. P., and Feher, G. (1988) *Proc. Natl. Acad. Sci. U.S.A. 85*, 9012−9016.
40. Plato, M., Lendzian, F., Lubitz, W., Trankle, E., and Mobius, K. (1988) *The Photosynthetic Bacterial Reaction Center: Structure and Dynamics* (Breton, J., and Vermeglio, A., Eds.) pp 379−388, Plenum Press, New York and London.
41. Vos, M. H., Lambry, J.-C., Robles, S. J., Youvan, D. C., Breton, J., and Martin, J.-L. (1992) *Proc. Natl. Acad. Sci. U.S.A. 89*, 613−617.
42. Gardner, K. H., and Kay, L. E. (1998) *Annu. Rev. Biophys. Biomol. Struct. 27*, 357−406.
43. Clayton, R. K. (1978) *Biochim. Biophys Acta 504*, 255−264.
44. Rafferty, C. N., and Clayton, R. K. (1979) *Biochim. Biophys. Acta 545*, 106−121.
45. Godik, V. I., Noks, P. P., Kononenko, A. A., Borisov, A. Yu., and Rubin, A. B. (1984) *Mol. Biol.* (*Moscow*) *18*, 1562−1568.

BI020250N